Journal of Physics: Conference Series **381** (2012) 012100 doi:10.1088/1742-6596/381/1/012100

Trends in the $g_{7/2}$ and $h_{11/2}$ neutron single-particle energies in $N = 51$ isotones

D K Sharp[1], B P Kay[2], S J Freeman[1], J P Schiffer[2], B B Back[2], T Bloxham[3], J A Clark[2], C M Deibel[2,4], C R Hoffman[2], A M Howard[1], J C Lighthall[2,5], S T Marley[2,5], A J Mitchell[1], P D Parker[6], J S Thomas[1], and A H Wuosmaa[5]

[1] Schuster Laboratory, University of Manchester, Manchester M13 9PL, UK
[2] Physics Division, Argonne National Laboratory, Argonne, Illinois 60439, USA
[3] Lawrence Berkeley National Laboratory, Berkeley, California 94720, USA
[4] Joint Institute for Nuclear Astrophysics, Michigan State University, East Lansing, Michigan 48824, USA
[5] Physics Department, Western Michigan University, Kalamazoo, Michigan 49008, USA
[6] A. W. Wright Nuclear Structure Laboratory, Yale University, New Haven, Connecticut 06520, USA

E-mail: david.sharp@postgrad.manchester.ac.uk

Abstract. The energies of the $g_{7/2}$ and $h_{11/2}$ neutron orbitals in $N = 51$ isotones have been investigated. The single-neutron adding reactions (d,p) and (α,^{3}He) have been performed on ^{88}Sr, ^{90}Zr and ^{92}Mo targets, at beam energies of 15 MeV and 50 MeV, respectively. These measurements were supplemented by studying the $d(^{86}\mathrm{Kr},p)^{87}\mathrm{Kr}$ reaction at an energy of 10 MeV/u, in inverse kinematics. Absolute cross sections were measured, ℓ assignments made and spectroscopic factors extracted. The energy centroids of the single-particle strength have been deduced and the observed trends are discussed.

1. Introduction

The single-particle properties of nuclei are fundamental to our understanding of nuclear structure. Recent findings in the structure of light nuclei have shown striking shifts in the shell structure far from stability. The disappearance of the $N = 20$ shell gap with the concurrent emergence of one at $N = 16$ is one example of such change [1]. Interest has been stimulated into investigation of the trends of single-particle states in chains of stable nuclei, especially where chains of isotopes or isotones are available. Recent measurements of the high-j states in the Sb isotopes via the (α,t) reaction have found systematic shifts of the $\pi g_{7/2}$ and $\pi h_{11/2}$ orbitals as the $\nu h_{11/2}$ orbital is filled [2]. Calculations combining a central potential and a tensor interaction between the neutrons in the $h_{11/2}$ orbital and protons in the $Z = 51$ nuclei have been shown to reproduce the observed shifts in energies [3]. Similarly, changes in the high-j orbitals in $N = 83$ isotones have been shown to shift in a manner consistent with the inclusion of the tensor interaction as the $\pi g_{7/2}$ orbital is filled [4, 5].

The $N = 51$ isotones provide another region in which to investigate trends in single-particle energies for varying neutron excess. Neutron-adding transfer reactions were used to populate states in ^{87}Kr, ^{89}Sr, ^{91}Zr and ^{93}Mo. The Fermi surface changes with mass across the chain

of isotones moving from the $fp-$shell, predominantly $j_<$ orbitals, to the $g_{9/2}$ orbital, a $j_>$ orbital. The tensor interaction is repulsive for like $j_>$ or $j_<$ pairs and attractive for $j_>j_<$ pairs. Thus a reversal of the effect due to the tensor interaction should be observed at $Z = 40$. The measurements in this work are aimed at a systematic study of the single-particle states in these $N = 51$ nuclei. The (α,^{3}He) and (d,p) reactions on the stable even $N = 50$ nuclei have been used; the momentum matching characteristics of these reactions allow a robust study of both high-j and low-j states.

2. Experiments

Measurements performed in normal kinematics

Measurements made in normal kinematics using the stable targets, ^{88}Sr, ^{90}Zr and ^{92}Mo, were made at the A. W. Wright Nuclear Structure Laboratory at Yale University. The Yale tandem accelerator delivered beams of 50-MeV α particles and 15-MeV deuterons. The outgoing ^{3}He ions and protons were momentum analysed using an Enge split-pole spectrometer which separates the ejectiles based on their magnetic rigidity. A position-sensitive gas-filled ionisation chamber and a plastic scintillator detector were positioned at the focal plane of the spectrometer. These detectors provided two energy-loss measurements which allowed for separation of different reaction channels using software gates.

Measurements were made at angles corresponding to the peaks of the distributions for transfer of $\ell = 0$, 2, 4 and 5 units of angular momentum. For the (d,p) reaction, these angles correspond to $\theta_{\rm lab} = 7°$, 18°, 34° and 42°, respectively. The peak of the $\ell = 0$ distribution is at 0° but due to experimental limitations 7° was used. The assumptions made in DWBA calculations are more valid at the peaks of the distributions so spectroscopic factors are more reliable at these angles. The angular distributions are all forward peaked in the (α,^{3}He) reactions so measurements were made at 5°. An extra angle was measured for the ^{90}Zr and ^{88}Sr targets, of 10° and 22.5° respectively, as broad contaminant peaks from reactions on ^{12}C and ^{16}O in the targets obscured a number of states in those spectra.

Spectroscopic factors are more reliable for reactions that have good momentum matching for the transfer of interest. For this reason, spectroscopic factors for $\ell = 0$ and $\ell = 2$ transfers are taken from the (d,p) measurements, whilst those for $\ell = 4$ and $\ell = 5$ are taken from the (α,^{3}He) reaction. In order to extract absolute cross sections, the product of target thickness and spectrometer entrance aperture was measured for each target. This was done using elastic scattering of α particles at 15 MeV at an angle of 20°. Under these conditions the elastic scattering is expected to be within 5% of the Rutherford prediction. The aperture was kept constant throughout the experiment in order to minimise systematic uncertainties. The beam dose was measured on a tantalum strip, located behind the target, connected to a Brookhaven current integrator.

Software gating was used to separate the protons and ^{3}He ions based on their energy loss characteristics. The focal plane spectra were then calibrated in excitation energy and yields extracted. The widths of fitted peaks in the spectra were fixed based on the determined widths of strong, isolated states. The observed resolution for the (d,p) spectra was ∼45 keV, whilst a typical (α,^{3}He) spectrum had a resolution of ∼90 keV. The measured energies in the (d,p) reactions were used to fix centroids in the (α,^{3}He) spectra which suffered from worse resolution. Once yields had been extracted and normalised to give absolute cross sections, they were fitted to angular distributions from DWBA calculations. The comparisons to the shape of DWBA calculations provided one means of assigning the amount of transferred angular momentum; the ratios between the two differing reactions provided another. High-ℓ transfers would have a larger cross section in the (α,^{3}He) reactions than the (d,p), with the converse being true for low-ℓ transfers due to the different momentum matching. Plotting the ratios of cross sections between the two reactions against two angles in the (d,p) reaction, such as in Fig. 1, provides

good separation of the different ℓ transfer as well as hinting at possible doublet states that appear with ratios that are inconsistent with the fitted angular distributions. Once assignments had been made, spectroscopic factors were extracted. These were taken as the ratio between the measured cross sections and those calculated using the DWBA code, PTOLEMY [6].

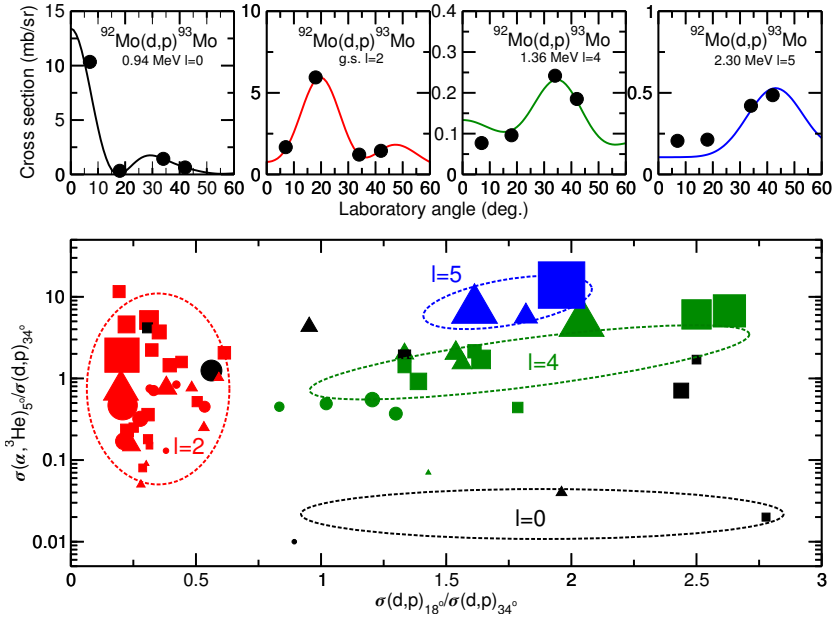

Figure 1. (Colour online) (Top) Representative (d,p) angular distributions with fitted DWBA calculations for $\ell = 0$, 2, 4, and 5. The cross sections and angles are given in the lab frame. The states are labelled by the excitation energy. (Bottom) The ratio of (α,^{3}He) to (d,p) cross sections measured at 5° and 34°, respectively, plotted against the ratio of cross sections measured at 18° and 34° in the (d,p). The size of the points are proportional to the (α,^{3}He) cross sections. The different angular momentum groups are circled and labelled. Circles, triangles and squares correspond to states in ^{89}Sr, ^{91}Zr and ^{93}Mo, respectively. Some $\ell = 0$ points lie out of the expected region although the angular distributions give $\ell = 0$ assignments: this is likely to be as a result of either higher-ℓ contaminants or higher order processes leading to an increased yield.

Measurement of the $d(^{86}Kr,p)^{87}Kr$ reaction

The $d(^{86}\mathrm{Kr},p)^{87}\mathrm{Kr}$ measurement was performed at the Argonne Tandem Linear Accelerator System (ATLAS) facility. A beam of ^{86}Kr was delivered by ATLAS at 10 MeV/u with an average intensity of 3×10^7 ions per second. The beam was incident along the magnetic axis of the HELIOS spectrometer, a large bore solenoid magnet, 235 cm in length and 92 cm in diameter [7, 8]. The beam was incident on a deuterated-polyethylene target positioned on the magnetic axis inside HELIOS. Emitted particles follow helical orbits in the uniform magnetic field, from the target, returning to the axis after one cyclotron period. The protons of interest, at $\theta_{\mathrm{c.m.}} < 50°$, are emitted in the backwards hemisphere of HELIOS. Before they return to the axis they are intercepted by an array of position-sensitive silicon detectors (PSDs) located around the beam axis. The array consists of 24 PSDs in a box configuration with six detectors on each side. Each detector has an active area of 9 mm by 50 mm and is 700 μm thick. For this measurement the array was situated -30 cm from the target, as measured from the nearest edge of the array, and had a centre of mass angle coverage of $\theta_{\mathrm{c.m.}}$ ~16–37° for protons populating

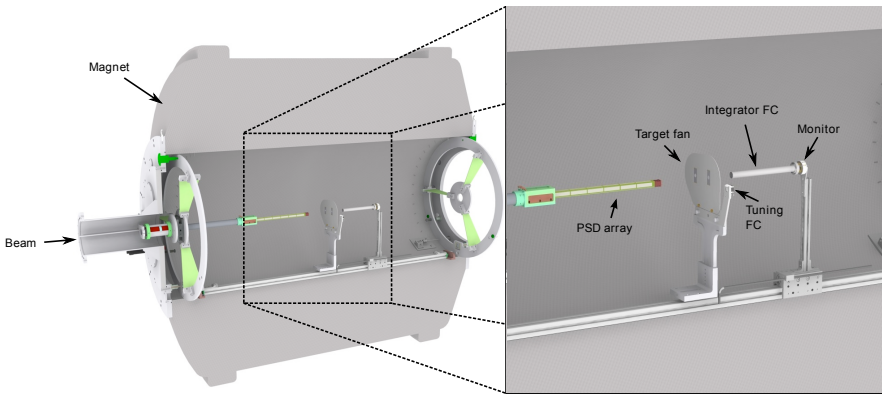

Figure 2. (Colour online)A schematic diagram of the HELIOS spectrometer. The inset shows a zoomed view of the arrangement of the target-array set-up. The major components are labelled. The distance between the PSD array and the target fan is variable and was positioned at $\Delta z = -30$ cm for this measurement. Adapted from Ref. [5].

the ground state of ^{87}Kr. The PSDs measure the proton energy and position from the target, Δz, and the time of flight relative to the radio frequency of the beam. A schematic of the arrangement of HELIOS can be seen in Fig. 2.

A plot of proton energy versus Δz is shown in Fig. 3 (a) for a single row of detectors. The energy was calibrated using a ^{228}Th α-particle source. The strong lines that can be observed correspond to protons populating states in ^{87}Kr. These data have been gated on the time of flight which corresponds to the cyclotron period of a proton. This removes background due to products from other channels, however there is still a contribution of protons from fusion-evaporation of the beam with the target. These protons are indistinguishable from protons from the (d,p) reaction. Each detector along a row corresponds to a different angular bin for each state, with the angle taken as that for the centre of the detector. In order to extract absolute cross sections the areal density of the target was measured using elastically scattered deuterons. These were detected by a Si monitor detector positioned at $\Delta z = 36$ cm corresponding to $\theta_{\mathrm{c.m.}} = 29°$. At 10 MeV/u, the elastic scattering cross section is expected to be within 50% of the Rutherford prediction. There was, therefore, a dependence of the measured thickness on the optical-model calculations used to obtain the elastic scattering cross sections. The thickness of the targets used was in the range 20–70 μg/cm^2. The beam dose was measured using an integrating Faraday cup positioned in front of the monitor detector. Both the position of the Faraday cup and monitor detector are shown in Fig. 2. The relative difference in efficiency of the PSDs was corrected for using the α-particle source, which should irradiate the detectors equally.

The kinematic lines, present in Fig. 3 (a), were straightened with respect to Δz and calibrated in terms of excitation energy. A representative excitation spectrum is shown in Fig. 3 (b). The observed excitation resolution varied from detector to detector in the range $\Delta E_x = 70$–130 keV. Yields were then extracted from the resulting spectrum for each detector and normalised using the measured areal density and beam dose to give an absolute cross section. The measured cross sections were compared to fitted angular distributions from DWBA calculations in order to make ℓ assignments. Examples of fitted angular distributions can be seen in Fig. 4.

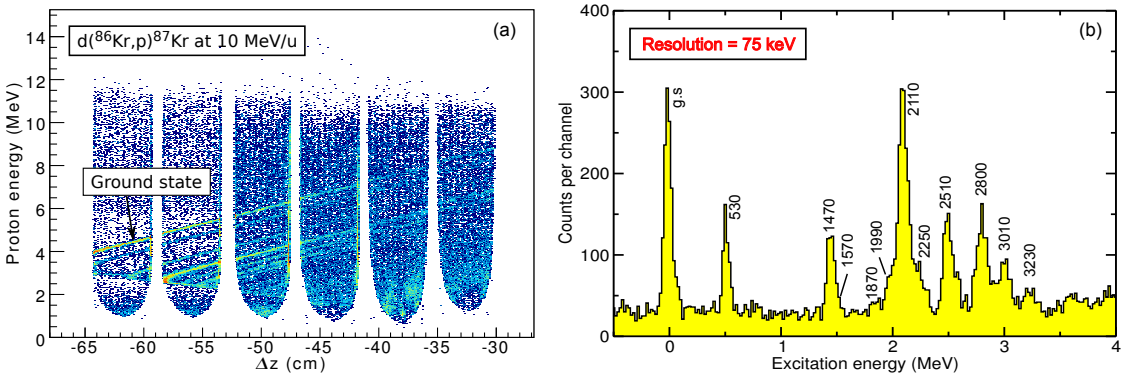

Figure 3. (Colour online) (a) An energy calibrated plot of proton energy against the target to detector distance, Δz, for the $d(^{86}\mathrm{Kr},p)^{87}\mathrm{Kr}$ reaction for one row of PSDs. The strong lines that are visible correspond to protons that have populated states in the residual nucleus. The kinematic line corresponding to population of the ground state has been labelled. These data have been gated on the cyclotron period for a single proton orbit. (b) A representative excitation spectrum for a single detector. States are labelled by their energy in keV.

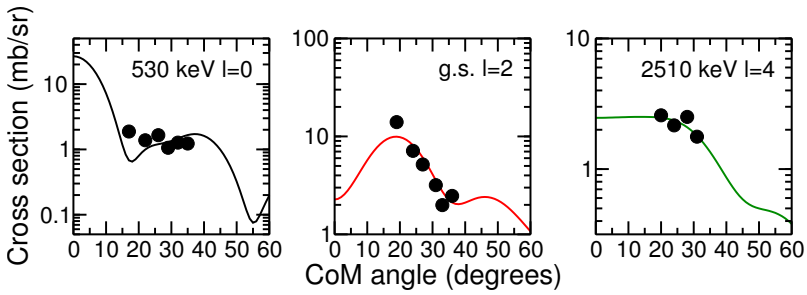

Figure 4. (Colour online) Representative angular distributions for the $d(^{86}\mathrm{Kr},p)^{87}\mathrm{Kr}$ reaction for $\ell = 0$, 2, and 4 transfers. DWBA calculations have been fitted to the measured cross sections (solid lines). The excitation energy of the states and the assigned ℓ are labelled.

3. Results

The spectroscopic factors for all observed states were extracted using a number of different optical-model parameters from Refs. given in [9]. A normalisation, N, was found for the spectroscopic factors by assuming $\Sigma NS = 1$ for each orbital. A common normalisation was found for all orbitals and across all the measured isotones for the (d,p) reaction, excluding the $\ell = 5$ transfers, as the strength of this transfer was found to be considerably less than the others. This may be due to increased fragmentation leading to a number of small fragments that were not identified above the continuum of states. The $(\alpha,^3\mathrm{He})$ spectroscopic factors were normalised based on the normalisation found for the $\ell = 4$ strength across all the isotones. The absolute spectroscopic factors were found to vary by ∼40% depending on the parameters that were chosen. However, the relative spectroscopic factors vary by only ∼15%. There is also a strong dependence of the absolute spectroscopic factors on the choice of bound-state parameters. A 5% change in the radius parameter, for instance, causes a 20–40% change in the spectroscopic factors. The bound-state parameters used in this analysis came from Refs. [10, 11] with a Reid potential used to calculate the deuteron bound-state wave function [12].

The centroids of the single-particle orbitals were calculated assuming $\ell = 0$, 4 and 5 transfers

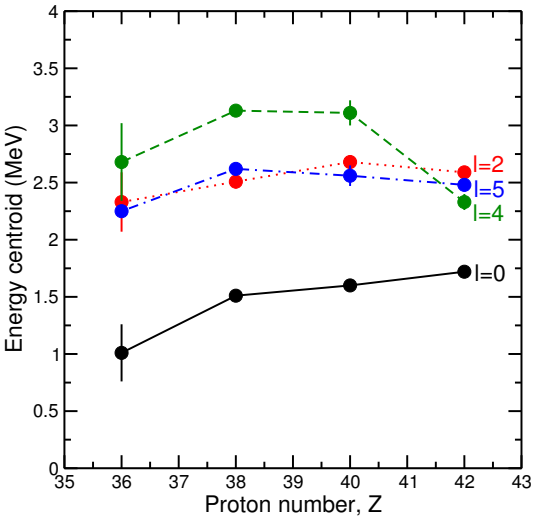

Figure 5. (Colour online)A plot of the excitation energy centroids as a function of proton number deduced for the $\ell = 0$ (black straight), 2 (red dotted), 4 (green dashed) and 5 (blue dash-dot) strength. These are preliminary results.

populate the $1s_{1/2}$, $0g_{7/2}$ and $0h_{11/2}$ orbitals. Transfer of $\ell = 2$ are assumed to populate the $1d_{5/2}$ and $1d_{3/2}$ orbitals. However, there is no way to distinguish between the two in these data. The reconstructed excitation-energy centroids are plotted in Fig. 5. With the filling of the fp-shell there appears to be an increase in the separation of the $g_{7/2}$ and $h_{11/2}$ (no $\ell = 5$ transfer was observed in ^{87}Kr) before a sudden reduction in the energy of the $g_{7/2}$ at $Z = 40$ brings these two energies closer together. This large reduction in the $g_{7/2}$ centroid could be attributed to the increase in the effect of the tensor interaction as the $g_{9/2}$ proton orbital is filled and appears to match the gradient of the trend as shown in Ref. [3]. The expected "flip" in the trends due to the tensor interaction appears to occur at $Z = 40$ due to the change from an occupancy of predominantly $j_<$ orbitals to the $j_>$ $g_{9/2}$ orbital. A more detailed discussion of this work is in preparation.

Acknowledgements

This work was supported by the UK Science and Technologies Facilities Council, the Engineering and Physical Sciences Research Council and the US Department of Energy, Office of Nuclear Physics, under Contract Nos. DE-FG02-91ER-40609 and DE-AC02-06CH11357.

References

[1] Ozawa A, Kobayashi T, Suzuki T, Yoshida K and Tanihata I 2000 *Phys. Rev. Lett.* **84**, 5493
[2] Schiffer J P *et al.* 2004 *Phys. Rev. Lett.* **92**, 162501
[3] Otsuka T, Suzuki T, Fujimoto R, Grawe H and Akaishi Y 2005 *Phys. Rev. Lett.* **95** 232502; Otsuka T, Matsuo T and Abe D 2006 *Phys. Rev. Lett.* **97** 162501; and Otsuka T *et al.* 2010 *Phys. Rev. Lett.* **104** 012501
[4] Kay B P *et al.* 2008 *Phys. Lett.* B **658**, 216
[5] Kay B P *et al.* 2011 *Phys. Rev.* C **84** 024325
[6] Macfarlane M H and Pieper S C 1978 *Argonne National Laboratory Report* ANL-76-11
[7] Wuosmaa A H, Schiffer J P, Back B B, Lister C J and Rehm K E 2007 *Nucl. Instrum. Methods Phys. Res.* A **580** 1290
[8] Lighthall J C *et al.* 2010 *Nucl. Instrum. Methods Phys. Res.* A **622** 97
[9] A total of 13 optical model parameter sets were explored, including those in: Perey C M and Perey F G 1963 *Phys. Rev.* **132**, 755; Becchetti F D and Greenlees G W 1969 *Phys. Rev.* **182**, 1190; An H and Cai C 2006 *Phys. Rev.* C **73**, 054605; Gales S *et al.* 1977 *Nuclear Physics* A **288**, 221; Bassani G and Picard J 1969 *Nuclear Physics* A **131**, 653; Bingham C R and Halbert M L 1970 *Phys. Rev.* C **2**, 2297
[10] Low K S and Tamura T 1975 *Phys. Rev.* C **11**, 789
[11] Satchler G R, Parkinson W C, and Hendrie D L 1969 *Phys. Rev.* **187**, 1491
[12] Reid Jr R V 1968 *Ann. Phys.* **50**, 411